

Fluid, hexatic, and crystal phases in terephthal-bis-(4*n*)-alkylanilines

D. Y. Noh, J. D. Brock, J. D. Litster, and R. J. Birgeneau

Department of Physics, Massachusetts Institute of Technology, Cambridge, Massachusetts 02139

J. W. Goodby

Department of Chemistry, The University of Hull, Hull HU6 7RX, England

(Received 20 March 1989)

X-ray scattering studies of single-domain samples of the terephthal-bis-(4*n*)-alkylanilines (TB*n*A) are presented. The growth of the bond orientational order parameters in the stacked hexatic S_F phase and the scaling relations between them are studied by analyzing the x-ray scattering profiles. The phase transition from the fluid S_C to the hexatic S_F phase changes from a discontinuous jump in TB5A to a continuous transition in TB7A. The S_F -to- S_G phase transition is first order. Results of a detailed analysis of the diffuse scattering from the S_G phase are reported.

MS code no. BC4267 1988 PACS number(s): 64.70.Md, 61.30.Gd

I. INTRODUCTION

During the past few years, significant progress has been made in the experimental study of both two- and three-dimensional hexatic phases. Such phases are characterized by order intermediate between that of an isotropic fluid and a crystalline solid. By studying rare gases physisorbed on various substrates,¹ arrays of ball bearings,² polyballs in water,³ and both lyotropic⁴ and thermotropic liquid crystals,⁵ the existence of a two-dimensional hexatic phase⁶ and a three-dimensional counterpart⁷ is no longer in question. Although there are now in the literature many experimental studies of hexatic phases, few measurements⁸ have concentrated on the critical behavior of the fluid-to-hexatic phase transition in a systematic way. Here we present a detailed x-ray scattering study of the fluid (S_C)-to-hexatic (S_F) phase transition in the terephthal-bis-(4*n*)-alkylanilines (TB*n*A) for $n=5,6,7$. The phase diagram for the TB*n*A series is qualitatively similar to that predicted by Aharony *et al.* (see Fig. 1).⁹ Studying this phase diagram was the original motivation for this work.

Previous experiments on other systems found the fluid-to-hexatic phase transition to be either continuous or weakly first order.⁸ If the transition is second order, one expects the specific heat to exhibit a singularity of the form $C_V \sim |t|^{-\alpha}$ where $t=(T-T_c)/T_c$ is the reduced temperature and α is the heat-capacity critical exponent. Interpreting heat-capacity data in this manner suggests that α is always large, of the order $\frac{1}{2}$, the value expected at a tricritical point. One proposed mechanism by which a tricritical point may be produced is to couple the bond orientational order parameter, Ψ_6 , to another order parameter. The effective free energy obtained by eliminating the additional order parameter from the partition function will contain a renormalized 4th order coefficient, which may change sign as the coupling strength is varied. Herringbone order,¹⁰ smectic layer fluctuations,¹¹ and crystal density fluctuations⁹ have all been suggested as candidates for the additional order parameter needed to

produce a tricritical point. Near the fluid-hexatic-crystal triple point, fluctuations in the crystalline order parameter may drive the originally second-order fluid-hexatic transition to first order. Moving away from the triple point, the effects of the crystalline order parameter fluctuations on Ψ_6 should decrease, returning the transition

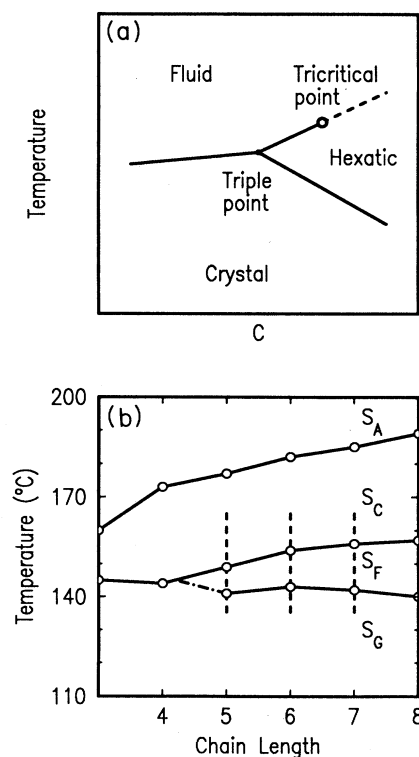


FIG. 1. (a) Generic temperature-concentration phase diagram near the crystal-hexatic-fluid triple point. The dashed (solid) lines indicate second- (first-) order transitions. (b) Temperature vs Alkyl chain length phase diagram of the TB*n*A series from Ref. 20. Data are taken along the dashed lines.

to second order and creating a tricritical point. The consequent phase diagram is illustrated at the top of Fig. 1.

In order to measure the hexatic order parameter, Ψ_6 , by x-ray scattering, a single-domain sample is crucial. Due to the large spot size in a typical x-ray experiment, orientational structure is averaged out in a multidomain sample. In the tilted hexatic phases, such as the S_F and the S_I phases, coupling between Ψ_6 and the molecular tilt field generates an effective ordering field,¹² allowing the production of a single-domain hexatic sample. This single-domain sample is obtained at the expense of formally breaking the symmetry we wish to study. In the weak-field limit, however, information about the critical behavior may still be obtained by considering the full equation of state.¹³ In our experiment, we measure the hexatic order parameter directly by Fourier analysis of the scattering function. The temperature dependence of the order parameter and the scaling relations among the Fourier coefficients enable us to study experimentally the region around the triple point.

The high-quality single-domain S_F samples produced in this experiment allow us to produce single-crystal S_G phase samples, by cooling very slowly through the $S_F \rightarrow S_G$ phase transition. The crystal axes are locked to the hexatic axes which are in turn well defined due to the hexatic order. Due to the relatively low resolution of this experiment, detailed information about positional correlations in the S_G phase is unobtainable; however, some features of the elastic properties of the S_G phase can be studied by analyzing the diffuse scattering in the wings of a Bragg peak. We find that the S_G phase has a large amount of diffuse scattering, indicating that the phase is very "soft."

The rest of this paper is organized as follows: In Sec. II, the experimental configuration and data are presented. In Sec. III, we review the harmonic scaling theory relating the various bond orientational order parameters. The analysis of the data taken on the fluid-to-hexatic transition is discussed in Sec. IV. In Sec. V, we present and analyze data on the S_G phase of TB6A and discuss its elastic properties.

II. EXPERIMENTAL RESULTS

For this experiment, we used primarily a low-resolution spectrometer configuration produced by using a cylindrically bent pyrolytic graphite (220) monochromator to focus vertically the Cu K_α emission line ($\lambda = 1.54 \text{ \AA}$) produced by an 18-kW rotating anode x-ray generator onto the sample. A flat graphite crystal served as an analyzer for the scattered x rays. The resulting k-space resolution ($\Delta Q = 0.01 \text{ \AA}^{-1}$, $\Delta\chi = 2^\circ$) was measured by placing a Si(111) crystal in the sample position.

The samples are freely suspended films of liquid crystal. The technique of preparing such films is described in detail in the references.¹⁴ The diameter of the films in this experiment is 6.375 mm and all of the films were $\geq 1 \text{ }\mu\text{m}$ thick. A 1-kG magnetic field produced by a pair of SmCo₅ magnets aligned the tilt field of the molecules at the $S_A \rightarrow S_C$ phase transition. Films were made in the

S_A phase at about 200°C, and annealed until uniform in thickness. Sample uniformity was determined by visual inspection. The sample chamber was kept at a pressure of 1 Torr; the residual gas was nitrogen. Temperature was controlled to $\pm 30 \text{ mK}$.

The scattering expected for two-dimensional fluid and hexatic phases is depicted schematically in Fig. 2. By scanning the angular variable χ , while staying on the peak of the fluid structure factor and the molecular form factor, one may probe the bond orientational order of the system.⁵ A representative χ scan and a longitudinal scan, taken deep in the S_F phase of TB6A where the bond orientational order has saturated are given in Fig. 3. The data exhibit well-defined peaks in the scattering at the χ positions expected for the S_F phase.¹⁵ Longitudinal scans through these peaks in the χ structure reveal that the positional correlation length is approximately 200 Å, demonstrating that, like the S_I phase,⁵ the S_F phase is indeed a stacked hexatic phase with long-range bond orientational order but short-range positional order. This agrees with the model of Ref. 7 and with the conclusions from previous experiments.¹⁵

At each point in a temperature sweep heating through

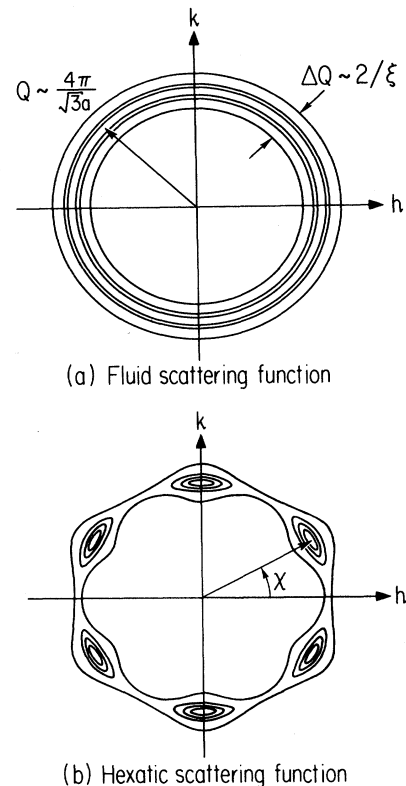


FIG. 2. (a) In-plane x-ray scattering profile expected for an isotropic two-dimensional fluid. The peak of the fluid structure factor is at roughly $4\pi/\sqrt{3}a$ where a is the interparticle distance. The width of the peak goes as $2/\xi$ where ξ is the distance over which positional correlations decay. (b) In-plane x-ray scattering profile expected for an ideal hexatic phase.

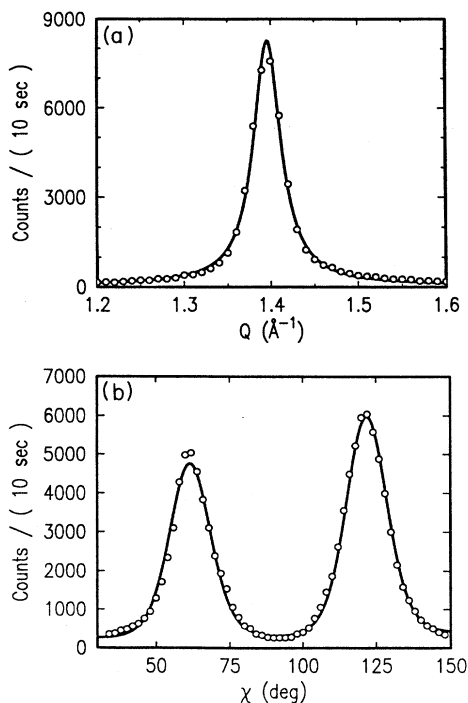


FIG. 3. (a) A longitudinal scan taken at $\chi = 120^\circ$ peak in the smectic- F phase. The solid line is fit to a power-of-Lorentzian line shape. (b) A χ scan which shows two peaks separated by 60° in the smectic- F phase. The solid line is the best fit to Eq. (1) using $\sigma_n = n + \lambda(T)n(n-1)$.

the $S_F \rightarrow S_C$ phase transition, we performed both χ and longitudinal scans through the peak at $\chi = 120^\circ$. Figure 4 shows χ scans at several temperatures passing through the S_F -to- S_C phase transition for TB5A, TB6A, and TB7A. At high temperatures, the χ scans are flat, consistent with an isotropic ring of fluid scattering. With decreasing temperature, the fluid ring begins to acquire a

sixfold modulation. The sharp peaks deep in the S_F phase indicate that hexatic axes are well aligned across the whole illuminated area. The transition region of the TB5A sample is only ~ 0.6 K wide whereas those of TB6A and TB7A are about ~ 2.5 K wide.

The amount of $6n$ -fold order present in the system can be measured quantitatively by fitting the χ scan data to the form

$$S(\chi) = I_0 \left[\frac{1}{2} + \sum_{n=1}^{\infty} C_{6n} \cos 6n(\chi - 120) \right], \quad (1)$$

where we truncate the series at $n = 10$, since Fourier components of the orientational structure with $n > 10$ are found to be smaller than the statistical measurement error. Before fitting, Eq. (1) was multiplied by the illuminated volume correction, $\cos^2 \theta^{-1}$, where θ is the incident angle of the x-ray beam, and an experimentally measured background function, $I_{BG}(\chi)$, was added to the product.

The temperature dependences of C_6 , C_{12} , and C_{18} for TB5A, TB6A, and TB7A are shown in Fig. 5. In all of the samples, the fundamental order parameter, C_6 , grows very rapidly and it is not possible to determine the order of the transition simply by observing $C_6(T)$. Fortunately, the higher harmonics grow more smoothly and provide a valuable visual check. There is a definite jump in all of the $\{C_{6n}\}$ in TB5A. In contrast, in TB6A and in TB7A, C_{12} and C_{18} appear to grow continuously within the temperature resolution of this experiment.

One very striking result is the complete absence of any measurable pretransitional bond orientational ordering in any of the samples. This is in marked contrast to the system⁵ racemic 4-(2-methylbutyl)-phenyl-4'-(octyloxy)-(1,1')-biphenyl-4-carboxylate, which is usually given the more convenient name 8OSI, where significant bond orientational order persisted well into the S_C phase. Apparently, the coupling between Ψ_6 and the molecular tilt

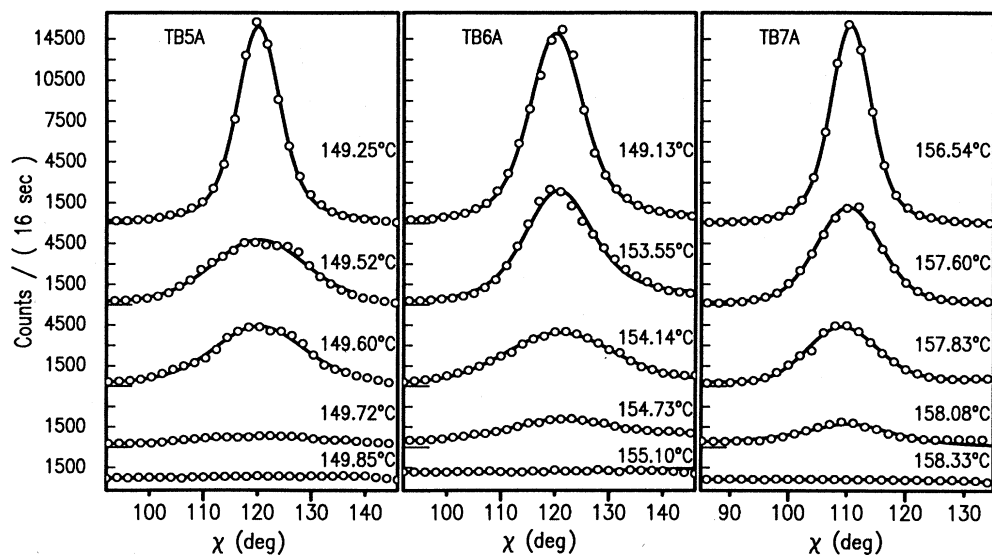


FIG. 4. Orientational scans at several temperatures across the S_F -to- S_C transition. The solid lines are the results of fits to the Fourier series assuming the scaling relations given by Eq. (6).

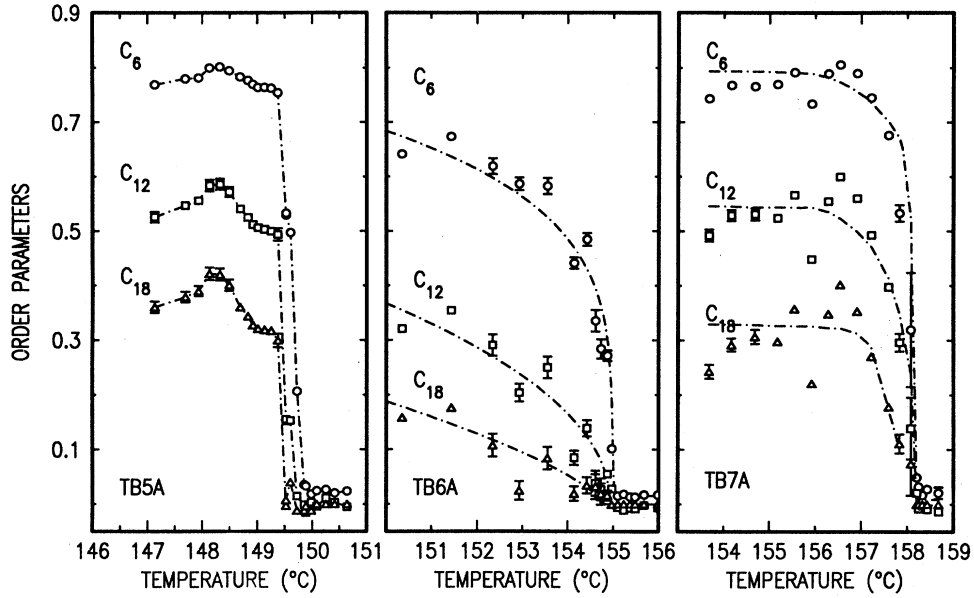


FIG. 5. First three Fourier coefficients describing the hexatic ordering for TB5A, TB6A, and TB7A as functions of temperature. Error bars represent a doubling of χ^2 . The lines are guides for the eye.

field is much smaller in the TBnA system than in the 8OSI system. Thus, the TBnA system is a better example of a weak-field limit system than 8OSI and better suited for phase transition studies.

III. REVIEW OF HARMONIC SCALING THEORY

In previous experimental work it was discovered that the harmonics of the fundamental order parameter scale as $C_{6n} = C_6^{\sigma n}$.⁵ This discovery inspired a renewed theoretical effort on the fluid-hexatic phase transition. To begin, we define the bond orientational order parameter using the definition of Aeppli and Bruinsma.¹⁷ The fluid is divided into microscopic cells of characteristic length Λ_0^{-1} , where Λ_0^{-1} is large compared to the liquid positional correlation length, ξ . In each of these cells V_r , where \mathbf{r} is the position vector, we calculate the Fourier-transformed density $\rho_q(\mathbf{r})$ for $|\mathbf{q}| > \Lambda_0$. Using $\rho_q(\mathbf{r})$, which has an infinite number of components indexed by \mathbf{q} , one can define a two-component vector field representing the hexatic order parameter:

$$\Psi_6(\mathbf{r}) = \Psi_6(\mathbf{r})e^{i6\theta(\mathbf{r})} = \int d\theta_{q_0} e^{i6\theta_{q_0}} |\rho_{q_0}(\mathbf{r})|^2, \quad (2)$$

where $|q_0|$ is the peak of the fluid structure factor. In an x-ray scattering experiment with $q = |\mathbf{q}| > \Lambda_0$, each cell scatters independently. The corresponding structure factor is

$$S(\mathbf{q}) = \int d^d r \langle |\rho_q(\mathbf{r})|^2 \rangle. \quad (3)$$

Therefore,

$$\begin{aligned} \int d\theta_{q_0} e^{i6\theta_{q_0}} S(\mathbf{q}_0) &= \int d^d r \int d\theta_{q_0} e^{i6\theta_{q_0}} \langle |\rho_{q_0}(\mathbf{r})|^2 \rangle \\ &= \int d^d r \langle \Psi_6(\mathbf{r}) \rangle. \end{aligned} \quad (4)$$

Similarly, we define an infinite set of bond orientational order parameters

$$\Psi_{6n}(\mathbf{r}) = \int d^d r \int d\theta_{q_0} e^{i6n\theta_{q_0}} \langle |\rho_{q_0}(\mathbf{r})|^2 \rangle \quad (5)$$

indexed by n . The C_{6n} defined in Eq. (1) are simply $C_{6n} = \text{Re} \int d^d r \langle \Psi_{6n}(\mathbf{r}) \rangle$, the real component of the spatial average over the illuminated spot size of $\text{Re} \langle \Psi_{6n}(\mathbf{r}) \rangle$.⁵

The fluid-hexatic phase transition theory begins with the Ginzburg-Landau-Wilson Hamiltonian,⁹

$$\begin{aligned} H = \int d^d x [& \frac{1}{2} |\nabla \Psi_6(\mathbf{x})|^2 + \frac{1}{2} r |\Psi_6(\mathbf{x})|^2 \\ & + u_4^0 |\Psi_6(\mathbf{x})|^4 + u_6 |\Psi_6(\mathbf{x})|^6 \\ & - h \text{Re} \Psi_6(\mathbf{x})]. \end{aligned} \quad (6)$$

For the special case $h=0$, this model exhibits XY-model critical behavior, provided that u_4^0 is larger than the tricritical value u_{4t} . The renormalized coefficient, u_4^0 is obtained by eliminating all other order parameters from the partition function. In the absence of fluctuations, $u_{4t} = 0$. However, fluctuations shift u_{4t} to negative values. Aharony *et al.*⁹ have argued that the fluid-hexatic-solid phase diagram should have the generic structure shown in the upper panel of Fig. 1. In this experiment, the system is not in the plane of Fig. 1(a) (i.e., $h \neq 0$). For an infinitesimally small field h , one expects the tricritical point to turn into a critical point, the second-order line to disappear and the first-order line to remain. At higher field strengths, the first-order transition line may also disappear as the critical point moves toward the triple point. The C_{6n} data shown in Fig. 5 indicate that there is no pretransitional, field-induced bond orientational order in these samples. Therefore, we assume that we may ig-

nore the effects of the ordering field.

If the system crosses the field-hexatic phase boundary in the second-order region, the scaling result of Aharony *et al.* applies.

$$C_{6n} = C_6^n [1 + (u_4/u_4^*) (C_6^{-2\epsilon/(d-2+\eta)} - 1)]^{-n(n-1)/10}. \quad (7)$$

Here $u_4^* = \pi^2 \epsilon / 5$ is the XY -model fixed point,¹⁸ and $u_4 = u_4^0 - u_{4t}$ is the distance from the tricritical point. Equation (7) is valid when C_6 is not too small. It is exact when $d=4$ and is also valid for dimensions $d \geq 3$ near the tricritical point where u_4 is small. Asymptotically close to the XY -model fixed point, Eq. (7) can be rewritten as

$$C_{6n} = C_6^{n+\lambda n(n-1)/(d-2+\eta)}. \quad (8)$$

An ϵ expansion predicts that in three dimensions $\lambda_n = 0.3 - 0.008n$.¹⁹ Both of these scaling forms, Eq. (7) and Eq. (8), predict that the correction to the mean-field result, $C_{6n} \sim C_6^n$, scales as a temperature-dependent term raised to the power $n(n-1)$. This suggests, in three dimensions, the scaling from $C_{6n} = C_6^{\sigma_n}$ where $\sigma_n = n + \lambda(T)n(n-1)$.

In a Landau theory, one assumes that the major temperature dependence is in the coefficient of the quadratic term. All other coefficients, including, in particular, u_4 , are taken to be independent of temperature. Therefore, using Eq. (7) we may measure u_4/u_4^* in the region where $C_6 \sim 1$. If $u_4 \sim 0$, the system is near a tricritical point. If the system does not happen to cross the $S_C - S_F$ phase

boundary in the second-order region of Fig. 1(a), the interpretation is slightly different. Scaling does not hold for a first-order transition; therefore, Eq. 7 does not apply. However, once the system is in the hexatic phase the structure is the same regardless of the order of the transition into the phase. Thus, Eq. (7) may be used to calculate the C_{6n} , but the identification of u_4/u_4^* as the Landau coefficient is no longer necessarily valid. In the critical region, Eq. (8) applies. In mean-field theory or at a tricritical point, $\lambda=0$, while $\lambda \sim 0.3$ is expected at the 3D- XY phase transition.⁹ One can determine whether or not a given system is tricritical by measuring the values of λ or equivalently u_4/u_4^* . At a tricritical point, $u_4=0$ and $\lambda=0$. For a first-order transition, we expect the Landau expansion parameter $\lambda < 0.3$ due to the decreased importance of fluctuations. u_4 is expected to be small for a first-order transition by the same argument.

IV. ANALYSIS OF THE HEXATIC-TO-FLUID PHASE TRANSITION

Deep in the S_F phase, where $C_6 \sim 1$, the χ scan data can be fit to Eq. (1) assuming the relation between the harmonics given by Eq. (7) to determine the ratio u_4/u_4^* . The TB7A system has an average $u_4/u_4^* = 1.5 \pm 0.4$ where the error is one standard deviation, whereas $u_4/u_4^* = 0.1 \pm 0.2$ for the TB6A sample. The smallness of u_4/u_4^* for the TB6A indicates that it is very close to a tricritical point. The TB5A result is $u_4/u_4^* = 0.5 \pm 0.3$. u_4/u_4^* as a function of temperature for each of the samples studied is illustrated in Fig. 6. The apparent growth of the ratio, u_4/u_4^* , near the phase transition is due to the breakdown of the assumption that $C_6 \sim 1$.¹⁶

To study the scaling behavior near the phase transition, we fit the data using Eq. (1) with $C_{6n} = C_6^{\sigma_n}$ where $\sigma_n = n + \lambda n(n-1)$. The solid lines in Fig. 3(a) and Fig. 4 are the results of such fits assuming this scaling relation. This form is, strictly speaking, only valid in the critical region. For TB5A and TB6A, λ is close to zero deep in the S_F phase, consistent with a mean-field, tricritical or first-order transition. The scaling relation can be approximated in this region as $C_{6n} = C_6^n$. As the system approaches the phase transition, λ grows. This behavior may indicate that the system is crossing over to the three-dimensional XY critical regime where λ has the approximate value 0.3. Unfortunately, λ cannot be well determined experimentally when the system is close to the phase transition. In that region C_6 is small and the contributions of the higher Fourier coefficients to the scattering become negligible. In the TB7A system, $\lambda = 0.3 \pm 0.05$, even deep in the S_F phase. The TB7A system thus stays in the three-dimensional XY critical region and there is never an indication of any crossover to mean-field behavior. $\lambda(T)$ is shown in Fig. 7 for all of the samples.

The value of λ for TB7A system is very close to that of 8OSI which shows another kind of hexatic phase, the S_I phase. The approximate scaling parameter λ for 8OSI is virtually constant as a function of temperature with the value 0.295 ± 0.02 .⁵ The scaling analysis in the three-

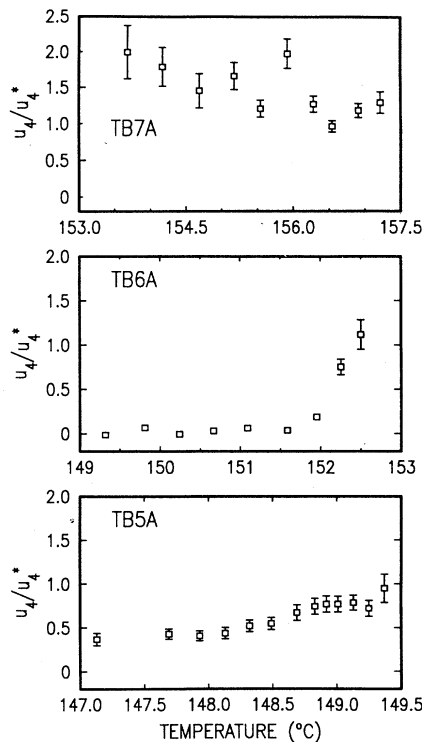


FIG. 6. Temperature dependence of u_4/u_4^* below the transition temperature from the fits which assume Eq. (5) for TB5A, TB6A, and TB7A. Error bars represent a doubling of χ^2 .

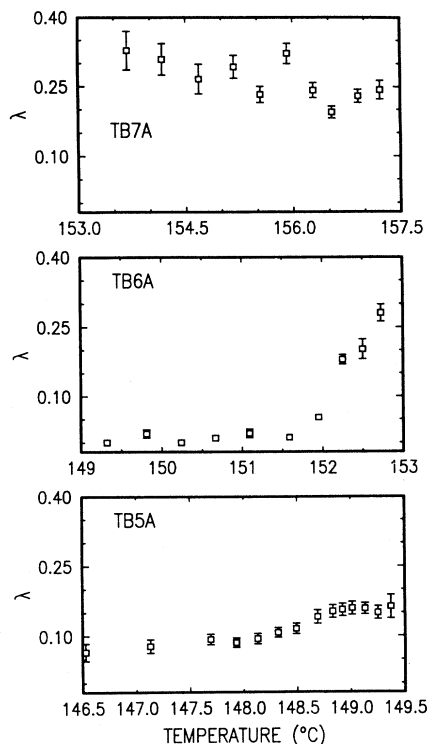


FIG. 7. Temperature dependence of λ for TB5A, TB6A, and TB7A. Note that λ is not experimentally well defined near or above the transition temperature.

dimensional XY critical region describes the two different tilted hexatic phases, S_F and S_I , amazingly well. The nature of the orientational fluctuations appear to be identical for S_F and S_I phases although they have different symmetry.

The order parameter curves, the values of the u_4/u_4^* 's and the λ 's consistently imply that a tricritical point should exist someplace near the TB6A system. However, the finite ordering field produced by the molecular tilt either formally destroys the phase transition or requires it to be first order. Therefore, the experimental paths drawn in Fig. 1(b) are not in the critical plane and the tricritical point is not accessible in a tilted system. Even though these systems are not in the critical plane, it is possible to observe the tricritical behavior or the crossover phenomena if they are close enough to the critical plane.

At the $S_C \rightarrow S_F$ phase transition, the smectic layer spacing undergoes a discontinuous jump. The size of the jump as a function of alkyl chain length has a minimum, close to zero, at roughly TB6A.²⁰ This is consistent with the observation that $C_6(T)$ grown most continuously in TB6A. The jump of the layer spacing and the growth of C_6 curve indicate that the TB7A system has a more first-order-like phase transition than the TB6A system. This is in contrast to the fact that the TB7A system shows the fluctuations of a three-dimensional XY system, while the TB6A apparently exhibits tricritical behavior.

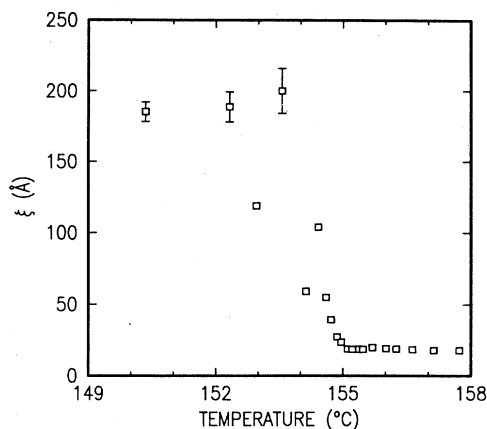


FIG. 8. Positional correlation length $\xi = \kappa^{-1}$ of TB6A obtained from the fits to SRL line shape.

The rapid narrowing of the longitudinal scans near the $S_C \rightarrow S_F$ phase transition indicates that the positional correlation length, ξ , increases rapidly. To analyze this effect quantitatively, one must use an explicit model. We have chosen a simple harmonic fluctuation model where the scattering is described as a mosaic average—due to the orientational fluctuations—of a two-dimensional Lorentzian fluid structure factor. In the limit of large fluctuations, this model predicts that a longitudinal scan will be described by a square root of a Lorentzian (SRL), while with no fluctuations, a longitudinal scan would be described by a simple Lorentzian. In the S_C phase, longitudinal scans are indeed well described by a SRL line shape; and, as expected, deep in the S_F phase the simple Lorentzian line shape works better. To interpolate between these two forms, we allowed the exponent of the Lorentzian to float between $\frac{1}{2}$ and 1. The exponent varied from ~ 0.5 at the phase transition to ~ 0.7 deep in the S_F phase. The solid line in Fig. 3(b) is the result of such a fit. Clearly this line shape works well. The positional correlation length, $\xi = \kappa^{-1}$, obtained from the SRL line shape for TB6A is plotted in Fig. 8. The rapid growth of ξ while C_6 is changing rapidly suggests that the growth in ξ is due to a coupling between the positional order and the bond orientational order.

V. THE CRYSTALLINE S_G PHASE OF TB6A

The $S_F \rightarrow S_G$ phase transition of TB6A is first order. Around 142°C, a sharp Bragg peak appears at the center of the hexatic peak. From the positions of the Bragg peaks, we confirm the previous experimental finding that the S_G phase is triclinic.²¹ The in-plane lattice spacing along the axes $\pm 30^\circ$ from the field direction is 4.52 Å and the layer spacing is 29.8 Å. The angle between the crystal axis and the smectic layer normal, γ , is $\sim 37^\circ$. γ is very close to the tilt angle of the molecules measured from the peak of the molecular form factor at the

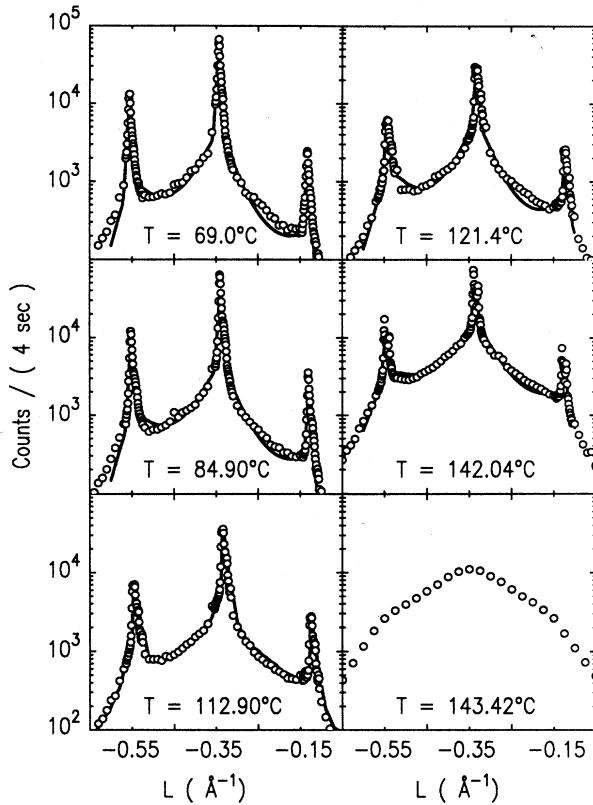


FIG. 9. Series of $(0,1,L)$ scans through the in-plane peak. The scan at $T=143.42^\circ\text{C}$ represents the molecular form factor since it is taken in smectic- F phase. The solid lines are the best fit to Eq. (13) convolved with the experimental resolution.

$S_F \rightarrow S_G$ phase transition and does not vary with temperature. The S_G phase exhibits the extremely rare AA layer stacking order, seen only in other smectic liquid crystals.^{14,16}

Due to the broad instrumental resolution of the spec-

$$S(\mathbf{Q}) = e^{-2W} |F(\mathbf{Q})|^2 \sum_{\mathbf{R}} e^{i\mathbf{Q}\cdot\mathbf{R}} \left[1 + \sum_{\mathbf{k}} e^{i\mathbf{k}\cdot\mathbf{R}} \sum_{i,j=1}^3 Q_i^2 \langle |u_j^i(\mathbf{k})|^2 \rangle \right], \quad (9)$$

where e^{-2W} is the Debye-Waller factor, $|F(\mathbf{Q})|^2$ is the molecular form factor, \mathbf{Q} is the scattering vector, and $\mathbf{u}(\mathbf{k})$ is the displacement vector of the phonon mode with wave vector \mathbf{k} . The index j runs over the three branches of the dispersion surface. Phonons with polarization vectors normal to \mathbf{Q} do not contribute to the diffuse scattering. In particular, in a $(0,1,\epsilon)$ scan, only those phonon modes with $\mathbf{k} \parallel [001]$ will contribute to the diffuse intensity.

Along the high-symmetry directions of the crystal, phonons can be classified as either pure longitudinal or pure transverse. Thus, if we let $\mathbf{Q} = (0,1,k)$, the above equation becomes

$$S(\mathbf{Q}) = e^{-2W} |F(\mathbf{Q})|^2 \frac{(2\pi)^3}{\Omega_0} \left[\delta(k) + \frac{V_0}{(2\pi)^3} [G_{010}^2 u_l^2(k) + k^2 u_t^2(k)] \right], \quad (10)$$

where Ω_0 is the volume of the unit cell. Here, G_{010} is the magnitude of $(0,1,0)$ and V_0 is the volume of the sample.

When temperatures are not too low, the equipartition theorem applies and

$$\langle |u(\mathbf{k})|^2 \rangle = \frac{2k_B T}{NM\omega^2(\mathbf{k})}, \quad (11)$$

where N is the number of molecules and M is the mass of a molecule. If we now assume dispersion relations of the form

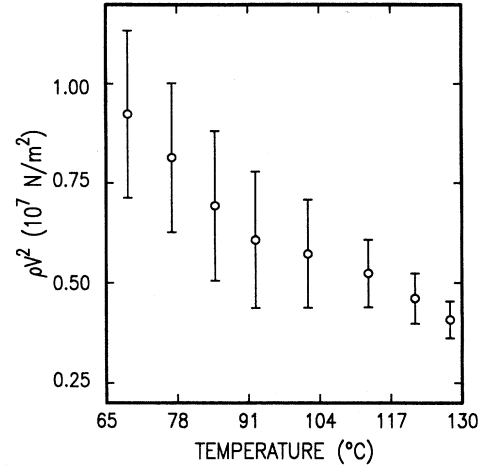


FIG. 10. The temperature dependence of the elastic constant, $\rho V^2(001)$, deep in the smectic- G phase.

trometer configuration, no information about the Bragg component of the scattering is obtainable; however, an unusually large diffuse component of the scattering allows the extraction of information about the elastic properties of the S_G phase. The diffuse scattering originates in the thermal vibrations of the crystal lattice.

Since each unit cell contains two molecules, in the limit of perfectly rigid molecules, there are three optical and three acoustic branches of the phonon dispersion surface. For simplicity, we ignore the distortion of the triangular lattice in the smectic plane and assume a simple hexagonal lattice structure. This simplification doubles the Brillouin zone, leaving only the three acoustic branches of the dispersion surface.

To include the effect of phonon modes, we include first-order thermal diffuse scattering in our line shape. This can be done simply in a harmonic theory,

$$\omega(\mathbf{k}) = V(\mathbf{k}) \frac{G}{\pi} \sin(\pi k / G), \quad (12)$$

where $V(\mathbf{k})$ is the velocity of sound in the $\mathbf{k}/|\mathbf{k}|$ direction, the scattering is given by the simple form

$$S(\mathbf{Q}) = e^{-2W} |F(\mathbf{Q})|^2 \left[\frac{(2\pi)^3}{\Omega_0} \delta(k) + \frac{2\pi^2 k_B T G_{010}^2}{\rho V_i^2 \Omega_0 G_{001}^2 \sin^2(\pi k / G_{001})} \right], \quad (13)$$

where the contribution of the longitudinal mode along the $[01k]$ direction is ignored since G_{010} is much greater than the magnitude of \mathbf{k} .

Due to the coarse resolution of the spectrometer configuration, we can compare the intensity of the Bragg component convolved with the resolution function to the intensity of the diffuse component of the scattering. Thus, we can estimate the absolute magnitude of the transverse sound velocity $V_i(001)$. The measured transverse resolution function is well approximated by a Gaussian of width 0.007 \AA^{-1} . Using a numerical integration, the measured scattering from a $(0, 1, \epsilon)$ scan was fit to the convolution of Eq. (13) and the assumed Gaussian resolution function. The $(0, 1, \epsilon)$ data and fits to Eq. (13) are shown in Fig. 9. As expected, the diffuse part of the scattering becomes smaller with decreasing temperature. The temperature dependence of the elastic stiffness constant, $\rho V_i^2(001)$, is plotted in Fig. 10.

As a last check on the positional order in the S_G phase, we changed the spectrometer to a high-resolution configuration using a Ge(111) monochromator and analyzer. The Bragg component of the scattering was still within the instrumental resolution indicating that the positional correlation length, ξ , is greater than 3000 \AA . Therefore, the S_G phase is a true three-dimensional crystalline phase but with elastic stiffness constants much smaller than those found in most other crystals.

VI. CONCLUSIONS

First, using a single-domain S_F sample, we have confirmed that the S_F phase is a three-dimensional,

stacked hexatic phase analogous to the S_I phase. The hexatic fluctuations of both the 8OSI (S_I) and the TB7A (S_F) systems are well described by a scaling analysis in the three-dimensional XY critical region. By studying the behavior of both λ and u_4/u_4^* as functions of alkyl chain length and temperature, we find indications of a tricritical point someplace nearby in the phase diagram. However, TB7A is clearly returning to first-order behavior, contrary to the hypothesis of Aharony *et al.*⁹ Thus, although the fluctuations behave as predicted, the transition itself does not. The growth of λ near the transition for the TB5A and TB6A systems suggests a possible crossover to three-dimensional XY critical behavior. After slowly cooling a single-domain S_F phase sample to obtain a single-domain S_G phase sample, we showed that the S_G phase is a true crystalline solid with long-range positional order but very soft elastic stiffness constants. The hexatic-to-solid transition is first order and the crystal has a triclinic structure with AA stacking order.

ACKNOWLEDGMENTS

It is a pleasure to acknowledge informative discussions with A. Aharony and J. O. Fossum. We are grateful to W. J. Nuttall for technical assistance. This research has been supported by the National Science Foundation—Materials Research Laboratory under Contract No. DMR 84-18718 and by National Science Foundation Grant No. DMR 86-19234.

- ¹S. E. Nagler, P. M. Horn, T. F. Rosenbaum, R. J. Birgeneau, M. Sutton, S. G. J. Mochrie, D. E. Moncton, and R. Clarke, *Phys. Rev. B* **32**, 7373 (1985).
- ²D. R. Nelson, M. Rubenstein, and F. Spaepen, *Philos. Mag.* **A46**, 105 (1982).
- ³C. A. Murray and D. H. Van Winkle, *Phys. Rev. Lett.* **58**, 1200 (1987).
- ⁴E. B. Sirota (private communication).
- ⁵J. D. Brock, A. Aharony, R. J. Birgeneau, K. W. Evans-Lutterodt, and J. D. Litster, *Phys. Rev. Lett.* **57**, 98 (1986); R. Pindak, D. E. Moncton, S. C. Davey, and J. W. Goodby, *ibid.* **46**, 1135 (1981). For general reviews see J. D. Brock, R. J. Birgeneau, J. D. Litster, and A. Aharony, *Phys. Today* **42** (No. 7), 52 (1989); *Contemp. Phys.* **30**, 321 (1989).
- ⁶D. R. Nelson and B. I. Halperin, *Phys. Rev. B* **19**, 2457 (1979).
- ⁷R. J. Birgeneau and J. D. Litster, *J. Phys. (Paris) Lett.* **39**, 1399 (1978).
- ⁸T. Pitchford, G. Nounesis, S. Dumrongrattana, J. M. Viner, C. C. Huang, and J. W. Goodby, *Phys. Rev. A* **38**, 1938 (1985).
- ⁹A. Aharony, R. J. Birgeneau, J. D. Brock, and J. D. Litster,

- Phys. Rev. Lett.* **57**, 1012 (1986).
- ¹⁰R. Bruinsma and G. Aeppli, *Phys. Rev. Lett.* **48**, 1625 (1982).
- ¹¹Jonathan V. Selinger, *J. Phys. (Paris)* **49**, 1387 (1988).
- ¹²D. R. Nelson and B. I. Halperin, *Phys. Rev. B* **21**, 5321 (1980).
- ¹³J. T. Ho and J. D. Litster, *Phys. Rev. B* **2**, 4523 (1970); A. A. Migdal, *Zh. Eksp. Teor. Fiz.* **62**, 1559 (1972) [*Sov. Phys.—JETP* **35**, 816 (1972)].
- ¹⁴J. Collett, L. B. Sorensen, and P. S. Pershan, *Phys. Rev. A* **32**, 1036 (1985).
- ¹⁵J. J. Benattar, F. Moussa, and M. Lambert, *J. Chim. Phys.* **80**, 99 (1983).
- ¹⁶J. D. Brock, D. Y. Noh, B. R. McClain, J. D. Litster, and R. J. Birgeneau, *Z. Phys. B* **74**, 197 (1989).
- ¹⁷G. Aeppli and R. Bruinsma, *Phys. Rev. Lett.* **53**, 2133 (1984).
- ¹⁸D. R. Nelson and J. Rudnick, *Phys. Rev. B* **13**, 2208 (1976).
- ¹⁹G. Jug, *Phys. Rev. B* **27**, 609 (1983).
- ²⁰Satyendra Kumar (private communication).
- ²¹E. B. Sirota, P. S. Pershan, L. B. Sorensen, and J. Collett, *Phys. Rev. A* **36**, 2890 (1987).